Research Article

Nano Research
2023, 16(5): 7646–7653

ISSN 1998-0124 CN 11-5974/O4
https://doi.org/10.1007/s12274-023-5439-y

Directional emissions from perovskite nanocrystals thin film enabled by metasurface integration through one step spin-coating process

Kexue Li[1,§], Xuanyu Zhang[2,§], Peinan Ni[3,§], Juncheng Liu[1], Fengyuan Lin[1], Xu Man[1], Wenfeng Cai[2], Jianxun Liu[2], Yanjun Liu[2], Rui Chen[2], and Zhipeng Wei[1] (✉)

[1] *State Key Laboratory of High Power Semiconductor Laser, School of physics, Changchun University of Science and Technology, Changchun 130022, China*
[2] *Department of Electrical and Electronic Engineering, Southern University of Science and Technology, Shenzhen 518055, China*
[3] *Photonics Laboratory, Department of Microtechnology and Nanoscience, Chalmers University of Technology, Göteborg, SE-41296, Sweden*
[§] *Kexue Li, Xuanyu Zhang, and Peinan Ni contributed equally to this work.*

Received: 31 October 2022 / **Revised:** 8 December 2022 / **Accepted:** 21 December 2022

ABSTRACT

Advances in thin film light-emitting devices have fueled the rapid growth of a new class of solid-state lighting devices, featuring low fabrication cost, high quantum efficiency, and broadband spectrum coverage, etc. In contrast to the conventional inorganic semiconductors that rely on lattice matched high crystalline quality substrate, solution processable thin films eliminate the dependence on the substrate, which is highly desired for the ease and versatility of integrations with foreign medium. By taking this advantage, this work developed an ultracompact solution to control the directionality of thin film emitters using integrated dielectric metasurface through one step spin-coating process. As a proof of concept, directional emissions from perovskite nanocrystal thin film, including collimated light emissions and two-dimensional beam steering, are experimentally demonstrated. Notably, our approach, where light emitters were integrated on the back side of substrate after the fabrication of metasurface, judiciously avoids any potential degradation of material optical quality caused by the multi-step nanofabrication. Therefore, it can serve as a generalized scheme to engage the advantageous properties of dielectric metasurface, including the compactness, high efficiency, and beam controllability with the emerging thin film light-emitting diodes (LEDs), which is applicable to a wide range of solution processable materials, including organic light-emitting diodes, quantum-dot light emitting diodes, polymer LEDs, and perovskite LEDs, opening up new pathways to develop low-cost and ultra-compact solid state light sources with versatile beams characteristics.

KEYWORDS

solid state light source, perovskite light-emitting diodes (LEDs), metasurface integrations, on-chip beam shaping, beam steering

1 Introduction

The emergence of solid-state lighting devices, known as semiconductor light-emitting diodes (LEDs), provides a new avenue to energy efficient lighting and displays with a variety of advantages over the traditional light sources, such as high quantum yields, compactness, good stability, and long lifetime [1, 2]. In contrast to the commonly used LEDs materials, i.e., the inorganic semiconductor materials that require rigorous growth conditions at high temperature in vacuum chambers, a new class of thin-film LEDs, including organic light-emitting diodes (OLEDs) [3], quantum-dot light emitting diodes (QLEDs) [4], polymer LEDs [5], and perovskite LEDs (PeLEDs) [6], stand out as an attractive platform for the development of low-cost and high-efficiency light sources, which features high photoluminescence (PL) quantum yield and simple preparation techniques using solution-based processing at room temperature [7–9]. However, the emissions of a typical thin-film LED manifest as a Lambertian-like beam profile with broad angular distributions and poor emission directionality due to the weak cavity effects. To solve this problem, beam shaping of the LEDs has grown into a vibrant research field with enormous potential to promote various emerging applications, such as visible light communications (VLC) [10], directional display [11], and photonic interconnects [12]. To date, conventional approaches to control the emission directionality of LEDs rely on the use of refractive optics. Nevertheless, since the refractive optical components utilize the phase accumulated during light propagation through media over a large distance, they are bulky and heavy, and require an external alignment process for integrations with LEDs, which inevitably increases the size and complexity of the device, and thus is not suitable for advanced applications where miniaturized optoelectronic systems are preferred. For instance, the current progress of near eye displays, such as virtual reality (VR) and augmented reality (AR), is suffering from the use of bulky and

Address correspondence to zpweicust@126.com

heavy collimating refractive lenses. Therefore, developing directional light source that can eliminate the need for a light collimator or optical combiners is highly desired, which will not only reduce the overall size of the display system but also improve the outcoupling efficiency of the light [11].

As a promising alternative, artificially designed planar optical structures, namely metasurfaces (two-dimensional (2D) equivalence of bulk metamaterials), are attracting considerable interest due to their exceptional capabilities to control the phase, amplitude, and polarization of the light by exerting local phase discontinuities within subwavelength dimensions [13–16]. The development of metasurface enables a new paradigm for the design of a wide range of ultra-thin optical devices, including flat lenses [17], waveplates [18], beam deflectors [19], polarization converters [20], and holograms covering a broad range of electromagnetic spectrum from THz to ultraviolet (UV) region. Despite the fast growth of metasurfaces based optical devices in the recent years, they mainly operate as stand-alone devices for free space applications. Notably, the exceptional characteristics of metasurfaces, such as the 2D planar configuration, ultra-compactness, lightweight, and complementary metal-oxide-semiconductor (CMOS) compatible fabrication process, are highly desirable for on-chip integrations with optoelectronic devices [21, 22]. In this context, important progresses have been made by integrating metasurface with both inorganic and organic LEDs to control and improve their emission properties. For instance, the polarization and direction of emissions from QLEDs can be controlled by directly structuring the top electrode into a nanoscale slot–groove–array structure [23], and the external quantum efficiency of commercial gallium nitride (GaN) LEDs can be improved by a factor of 1.65 by depositing a layer of disordered silver nanoparticles on top [24]. However, the intrinsic Ohmic loss associated with the plasmonic nanostructure has raised wide concerns for their practical applications. By contrast, the lossless nature of dielectric metasurface based on high index materials has demonstrated remarkable advantages for high-efficient operations. In this regard, integrations of dielectric metasurfaces have been successfully deployed in various inorganic semiconductor LEDs, including GaN LEDs [25], GaP LEDs [26], and GaAs LEDs [27], to control their emission properties, such as beam direction, polarization, and extraction efficiency, which covers a broad range of spectrum regions from green to near infrared. But since fabrications of dielectric metasurface heavily involve multiple cleanroom processes including the deposition, patterning and removal of hard mask, growth, and dry etching of dielectric material, directly integrating metasurface with solution synthesized materials like perovskites inevitably increases the risks of performance degradation due to their susceptivity and vulnerability to the harsh chemical environment. To overcome this limitation, it appears to be a practical and rather simple solution to fabricate metasurfaces prior to the integration of the light emitters. For instance, by transferring the as-grown perovskite microwire onto a TiO_2 metalens using polydimethylsiloxane (PDMS) space and proper alignments, Dai et al. demonstrated good collimation of the left-handed circularly polarized emission with a low divergence angle (< 0.9°) [28].

Here, by taking advantage of metasurface integration, we exploit on-chip beam shaping of solution processable thin film emitters using perovskite nanocrystals (PeNCs) as an example. We demonstrate that interfacing perovskite light source with beam shaping dielectric metasurfaces can be achieved through a rather simple step of spin-coating process without the risks of compromising its optical quality, which could serve as a compact and practical solution to control the wavefront of the emitting beam into versatile functionalities. Capitalizing on this concept, directional emissions, including on-chip generation of both collimating beam and deflecting beam, are realized from PeNCs thin films in the green spectral regime. Furthermore, we show that our approach enables the implementation of metalens-assisted 2D beam steering of thin-film based LEDs emissions in a simple fashion, which could find applications for dynamic control of outgoing beams in real time.

2 Results and discussion

2.1 Conceptual design and integration approach

Owing to their excellent photostability, core–shell $FAPbBr_3/CsPbBr_3$ nanocrystal PeNCs thin films were employed as the light emitters based on the same synthesis steps developed in our previous study [29]. To construct the dielectric metasurface that is suitable for the integration with PeNCs thin films, epitaxially grown high-quality GaN was employed in this work due to its high transmission efficiency, negligible absorption, and large refractive index in the whole visible regime, which ensures the high efficiency of wavefront control (see Fig. S1 in the Electronic Supplementary Material (ESM)). Experimentally, 1 μm thick GaN layer with small surface roughness was grown on a double side polished sapphire substrate via metalorganic chemical vapor deposition (MOCVD), as confirmed in Fig. S2 in the ESM. For the design of metasurface, nanopillars with circular cross-section were deployed as the building block of the integrated metasurface. Since this type of meta-atom can operate as a truncated waveguide, in which the effective refractive index of the propagation modes can be easily modulated by changing its dimension, it provides an effective platform to implement polarization insensitive phase control of the transmitted light [30]. Specifically, the complex transmission coefficients of the GaN nanopillar as a function of the radius were numerically investigated at the wavelength of 515 nm close to the PL peak of the as-grown PeNCs thin film by the difference time domain (FDTD) approach, where periodic boundary conditions were applied along all the in-plane directions and perfectly matched layer (PML) boundary condition was used in the direction of the light propagation. As evidenced in Fig. 1(a) that a complete phase modulation in 2π range with high transmission efficiency (> 80%) can be achieved by simply tuning the radius of the nanopillar from 65 to 100 nm, revealing the suitability of the selected meta-atoms for high efficiency beam shaping. For simplicity and without loss of generality, five nanopillars with different radii of 65, 74, 81, 86, and 93 nm were employed to build the meta-atom library in our design, which can introduce equally spaced phase retardation in range from 0 to 2π and satisfy the Maréchal's criterion such that the performance of the discretized metasurface is limited only by the diffraction of the light [31].

To elucidate the principle of on-chip beam shaping of PeNCs emitters, metasurface collimators with different focal length (f) were designed to impose the light emitted from a PeNCs thin film with a hyperboloidal phase delay

$$\phi_{\text{collimator}}(x,y) = 2\pi - \frac{2\pi n}{\lambda}\left(\sqrt{x^2+y^2+f^2} - f\right) \quad (1)$$

as depicted in Fig. 1(b), where n is the refractive index of the sapphire substrate, to compensate the spherical wavefront of the incoming beam for collimated emissions. To optimize the collimation performance, different focal lengths, f = 350, 390, 430, and 470 μm, were adopted in the design of metalenses such that the focal plane would be close to the back-side surface of the sapphire substrate when the incident green light shines from the metasurface side, considering the uncertainty of the nominal

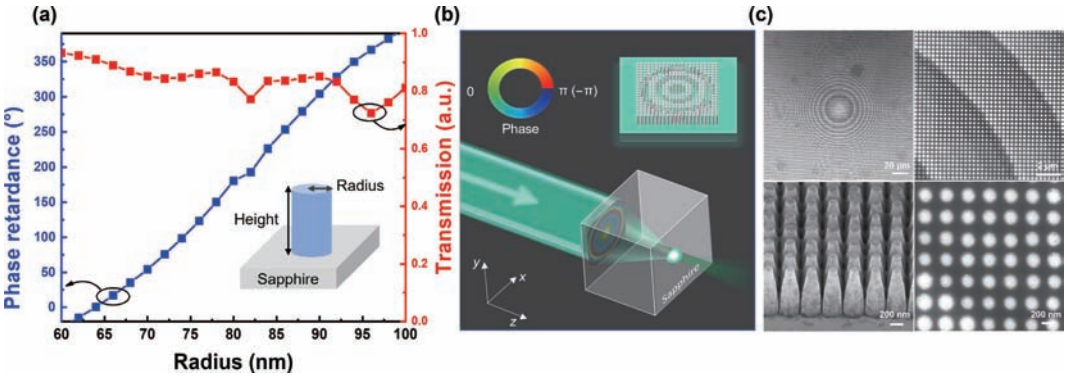

Figure 1 (a) Numerically calculated phase retardance and transmission of light at a wavelength of 515 nm scattered by GaN nanopillars with varying radii. The inset illustrates the nanopillar unit of the array, which is assembled in a subwavelength lattice of 340 nm at a double-side polished sapphire substrate. (b) Schematic illustration of the focusing characteristic of the designed metasurface collimator, in this example the incident green laser is focused on the back-side surface of the sapphire substrate. (c) Scanning electron microscopy (SEM) images of the fabricated GaN metasurfaces reveal their good morphology.

thickness of the sapphire substrate (430 ± 30 μm). Accordingly, the grown GaN layer was sculptured into an array of circular shaped nanopillars with a fixed subwavelength lattice constant of 340 nm and spatially varying radii (see the Methods section for fabrication details). The high accuracy of the developed fabrication technique can be confirmed by the well-defined surface morphology of the fabricated GaN metasurface (Fig. 1(c)).

Prior to the integration of PeNCs thin film, the focusing characteristics of the fabricated metalens were investigated using a homemade optical setup (see the Methods section and Fig. 2(a) for measurement details). In experiment, a collimated green laser with a wavelength of 532 nm, close to the design wavelength, was employed as the incident light source to examine the focal length of the metalenses in the spectral region of interest. The beam intensity profiles of the transmitted light were measured along its propagation direction after passing through the metalenses, as summarized in Fig. 2(b), where well-defined focal points can be observed at different positions, respectively. The measured focal lengths of samples S1, S2, and S3 show reasonable agreement with the design, while that of S4 exhibits a prolonged focal length (~ 498 μm) due to the change of the background refractive index from the sapphire substrate to the air. Figure 2(c) reveals that all the focal spots exhibit the full-width half-maximum (FWHM) values close to the diffraction-limited values (λ/2NA), where NA is the numerical aperture. Figure 2(d) presents the beam patterns of the 532 nm green laser measured directly on the back-side surface of sapphire substrate after passing through the metasurfaces, where a tightly focused point can be observed from the metasurface sample S3 with a focal length f = 430 μm. Therefore, the well-defined focusing properties of the metalenses, of which the focal plane locates close to the substrate, make them suitable to collimate the emitters placed at the back surface of substrate.

In particular, the good chemical and mechanical stability of the dielectric metasurfaces offer superior advantages for harsh environment applications and optoelectronic integrations over their polymer or metal-based counterparts [32, 33]. By combining such merits of dielectric metasurface with the solution processable manufacture of perovskite, we developed a feasible and simple approach to implement on-chip integration of dielectric metasurface with perovskite thin film through one step spin-coating process (see the Methods setion and Fig. 3(a) for details). Note that operations of beam shaping metasuface conventionally rely on the illumination of a spatially coherent source, whereas the low spatial coherence of the Lambertian-shaped emissions from a typical LED becomes problematic for effective beam control if the metasurface was integrated in close proximity to the emitter within several wavelengths range [34]. To overcome this limitation, Khaidarov et al. introduced a resonant Fabry–Perot (FP) cavity into the LED structure to improve its spatial coherence, and then controlled the LED emission by directly integrating the dielectric metasurface on top of a GaP LED [26]. Nevertheless, this approach requires additional fabrication steps of resonant cavity, which inevitably increases the overall fabrication complexity and cost. In contrast, our approach features the ease of integration, and offers several advantages: Firstly, since the thickness sapphire substrate is several orders of magnitude larger than the wavelength of incident light, it would spontaneously serve as an ideal beam expansion layer to greatly expand the light emissions from the integrated perovskite thin film before they reach the metasuface. By doing this, the perovskite emitter can be treated as a point source with respect to the metasurface, which not only helps to simplify the design of metasurface, but also relieve the constraint of the intrisically incoherent spontaneous emissions of perovskite LED on the beam shaping performance enabled by the metasurface. Secondly, different from the previous metasurface integration with LED where the metasurface was directly fabricated on top of the LED emitting surface, this work adopts a reverse structure by first defining the metasurface at one side of the substrate, and then integrating the emitter on the other side. Therefore, this configuration avoids any post-nanofabrication over the active region, which is particularly beneficial for the use of emitters that are sensitive and vulnerable to the harsh chemical environment. Thirdly, the developed integration approach where the light emitters can be treated as point sources can be readily scaled up for the purpose of beam shaping of micro-LEDs array. It thus enables a feasible and simple solution to implement metalense-assisted 2D beam steering of micro-LEDs in real time.

2.2 On-chip collimation of perovskite emissions with integrated metasurface

To testify the collimation performance of the integrated structures, the PL properties were measured under the excitation of a 355 nm UV laser, as illustrated in Fig. 3(b) (see the Methods section for details). Figure 3(c) summaries the PL intensity from different perovskite samples with and without metasurface integration, which was recorded and normalized as a function of the propagation distance. As evidenced, the emission intensity of the metasurface integrated PeNCs thin films remains nearly constant along its propagation direction up to 1 mm, while that of the bare PeNCs sample without metasurface rapidly drops to the background noise level after passing through the backside surface of the substrate. The PL spectra of different samples were measured and compared at Z = 1.3 mm, as shown in Fig. 3(d). Similar PL peak wavelength and FWHM were observed from all the as-grown PeNCs thin films, which revealed their comparable chemical composition and material optical quality. Notably, the

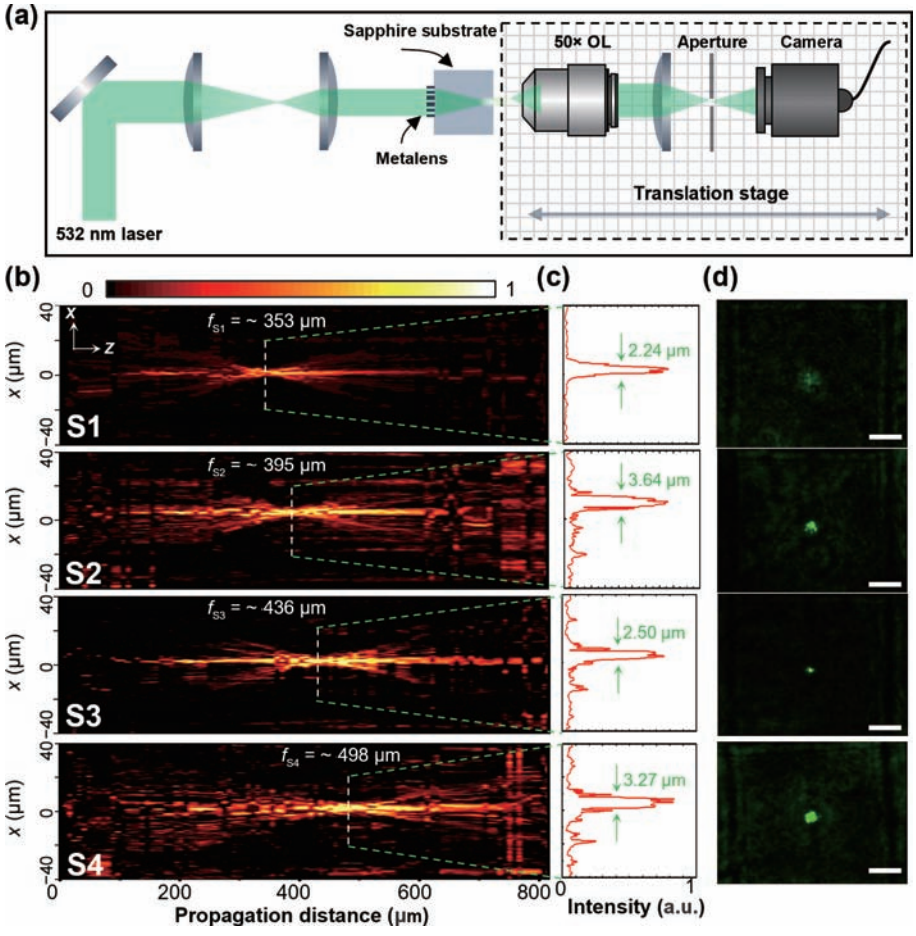

Figure 2 (a) Experiment set-up for beam profiles measurement. A CCD camera is mounted on a translation stage with a repeatable movement precision of 1 μm to record the transverse intensity distribution at different propagation distance. (b) The measured beam intensity distribution of a 532 nm laser after passing through the metasurfaces, where well-defined focal points can be observed in good agreement with the design. (c) The FWHM values of the intensity profiles at the foci are close to the diffraction-limited values, revealing the tight focusing properties of the obtained metalenses. (d) Beam patterns of the incident 532 nm laser directly measured at the backside surface of the sapphire substrate after passing through the metasurfaces, where a tightly focused point can be observed from the metasurface sample S3 with a focal length f = 430 μm, indicating that the actual thickness of the sapphire substrate is around 430 μm. The scale bar is 5 μm.

metasurface integrated sample S3 with f = 430 μm exhibits the strongest PL emission intensity, indicating the actual distance between the PeNCs emitter and the metasurface is close to 430 μm. Moreover, the collimation performance of the metasurface integrated sample was further evaluated by the comparison of angular distributions of the emission power from the PeNCs thin films with and without metasurface integration, as summarized in Fig. S3 in the ESM. It can be seen that the emission directionality of the metasurface integrated PeNCs emitter was significantly improved, in which 60% of the total emission power was concentrated within an angular range from −20.8° to 20.8°. In contrast, the emission from the bare PeNCs thin films without metasurface exhibits a broader angular distribution, where the same percentage of emission power spreads from −35.8° to 35.8°.

It is worth noting that despite the metasurface collimators were designed based on the dispersive propagation phase mechanism at the specified wavelength that is close to the spontaneous emission peak of the as-grown PeNCs, both the phase response and the transmission characteristics of the meta-atoms only exhibit small variations within the wavelength range from 515 to 535 nm, as revealed in Fig. S4 in the ESM, which allows operating the metasurface with comparable performance in this spectral region. This feature is particularly beneficial to ensure that the bandwidth of the integrated metasurface collimator with the same design is sufficient to cover different emission frequencies of the as-grown PeNCs according to the emission spectra, and thus mitigate any perturbation caused by the wavelength drifting, for example, due to the variation of the environment temperature, change of excitation conditions, and the transition from spontaneous emissions to the amplified spontaneous emissions (ASE) under higher excitation as shown in Figs. S5(a) and S5(b) in the ESM. To prove this concept, the light emitting characteristics of the samples were further studied by increasing the pumping power above the threshold of ASE (~ 340 nJ/cm^2), such that both strong spontaneous emission (around 515 nm) and ASE (peaked at 525 nm) can be observed (see Fig. S5 in the ESM). Accordingly, the total emission power of different PeNCs samples that contains both the spontaneous and ASE emissions was measured and compared along the light propagation direction, as shown in Fig. 4(a). It shows that the metasurface integrated PeNCs thin film S3 with f = 430 μm exhibits rather stable output power as the emitting light propagates from the surface, which agrees well with the observation in Fig. 3(c).

In contrast, the emission power from the PeNCs sample without metasurface integration dissipates quickly along the propagation direction. The good collimation performance is further confirmed by the measurement of the far-field beam patterns from different samples, as compared in Fig. 4(b) (see Fig. S6 in the ESM for measurement details). It is found that the emitting beam profiles from the metasurface integrated samples manifest as well-defined square patterns, which were determined by the actual shape of metasurface, whereas only a diffused and rather dim beam was observed from the bare PeNCs sample without metasurface integration. In addition, the emission spectra

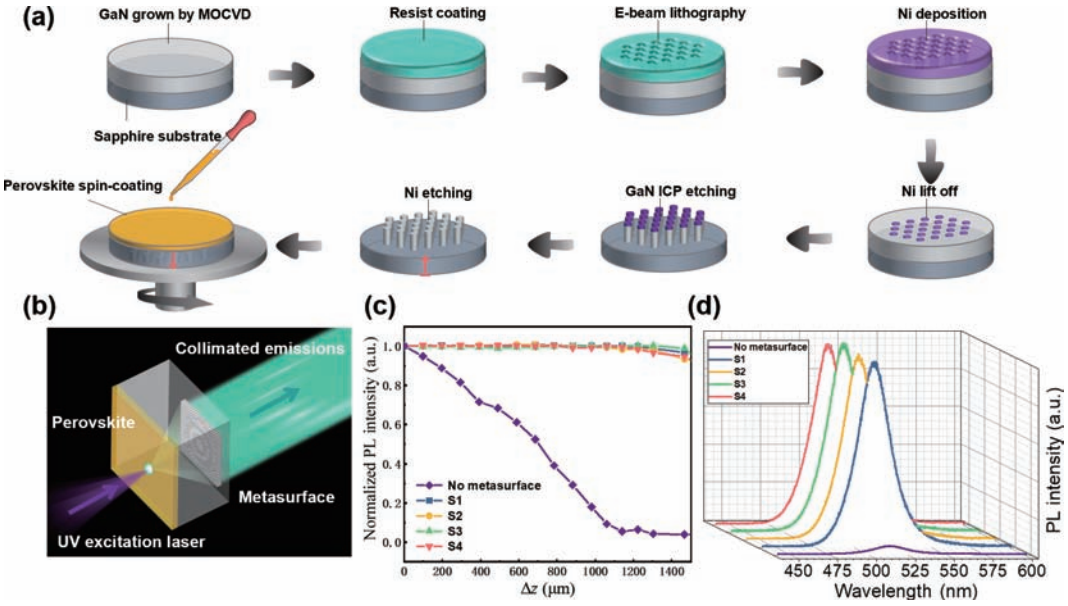

Figure 3 (a) The developed processes to integrate perovskite thin film (~ 100 nm in thickness) with GaN based dielectric metasurfaces. (b) Schematic of the proposed on-chip collimation of perovskite emissions using integrated metasurface collimator, where the perovskite emitter was placed at the focal plane of a metalens and pumped by a 355 nm nanosecond UV laser with the pulse width of 1.7 ns. (c) Measured PL intensity with and without metasurface as a function of the propagation distance under the excitation power of 0.3 mW. The output emission intensity of the collimated samples remains almost constant along the propagation direction up to 1 mm, while that of the bare laser decreases rapidly to the background noise. (d) PL spectra of different samples measured at Z = 1.3 mm, revealing that the metasurface integrated sample S3 with f = 430 μm exhibits the best collimation performance.

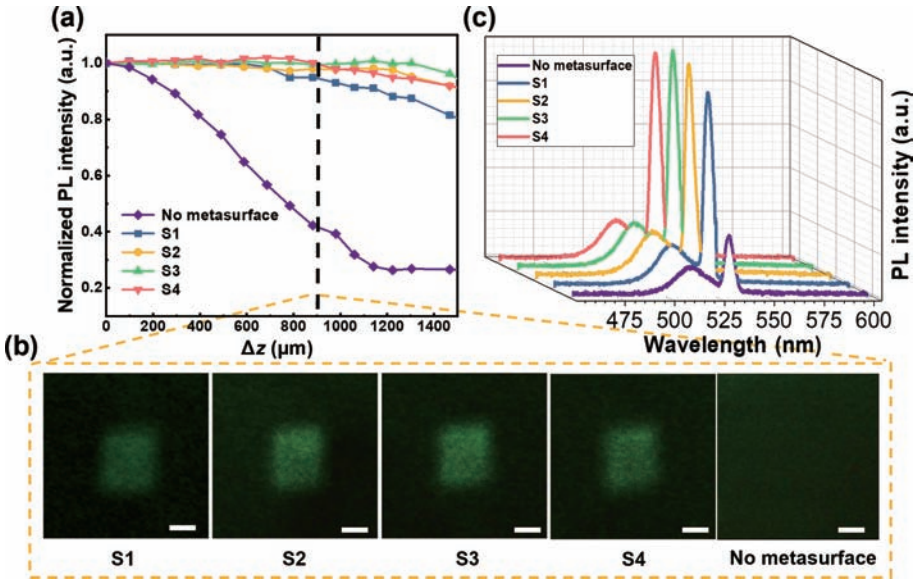

Figure 4 (a) PL intensity distributions of the samples with and without metasurface under the excitation power of 1.0 mW above the threshold of ASE along the propagation distance. Good collimation performance can be observed from the metasurface integrated samples. (b) Far-field beam patterns recorded at Z = 0.90 mm, where well-defined square patterns determined by the actual shape of metasurface can be observed, whereas only a diffused and rather dim beam is shown from the bare perovskite sample. The scale bar is 200 μm. (c) PL spectra of different samples were measured and compared at Z = 1.3 mm, confirming that the metasurfaces integrated samples show both enhanced spontaneous and ASE emissions compared with the bare perovskite sample.

of different samples were analyzed at the same propagation distance of Z = 1.3 mm, as shown in Fig. 4(c), which reveals that the metasurfaces integrated samples show both enhanced spontaneous and ASE emissions compared with the bare PeNCs sample. The above results validate the effectiveness and robustness of the collimation performance of the metasurface integration against the wavelength shifting of the PeNCs emitters caused by the variation of excitation conditions.

2.3 Metalens-assisted 2D beam steering of perovskite emissions

In the above example, the PeNCs thin film was utilized as a point source emitter located at the focal point of the integrated metalens for collimation purpose. It is worth noting that the developed metasurface integration approach is also able to control the beam profiles of the PeNCs emitters array located within a larger spatial region, which can be leveraged to develop thin film based micro-LEDs array with directional beam functionalities. By taking advantages of the high material quality of the as-grown perovskite thin film, we further demonstrate that the integrated metasurface is suitable for ultracompact beam steering of perovskite emissions. In particular, both the good thickness uniformity (Fig. S7 in the ESM) and optical homogeneity (Fig. S8 in the ESM) of the obtained PeNCs thin film ensure that high performance emitters array with comparable emitting characteristics can be realized from the PeNCs thin film. Moreover, the excellent light emitting stability of the obtained PeNCs emitters was proved by the time

revolved PL measurement, as shown in Fig. S9 in the ESM. The above characteristics of the PeNCs thin film are highly desirable to implement large-scale micro-LEDs array for advanced applications, such as high-resolution displays and free-space optical communications.

The discussion in the previous section reveals that the PeNCs thin film locates at the focal plane of the integrated metalens with f = 430 μm for sample S3. Therefore, this specific configuration allows the light emitted at a given position (x, y) in the plane of the PeNCs thin film to be collimated and deflected with a well-defined deflection angle of $\theta(x, y)$ after passing through the metalens, as illustrated in Fig. 5(a), where $\theta(x, y)$ can be approximately given by

$$\theta(x,y) = \tan^{-1}\left(\frac{n_{\text{air}}\sqrt{x^2+y^2}}{n_{\text{sapphire}}\cdot f}\right) \quad (2)$$

Moreover, the light from PeNCs emitters located at different positions in this structure will intersect out-plane at the same point (denoted as "P") as if the "P" point was behaving as a virtual light source, of which the emitting beam can be continuously steered by a specific angle θ (Fig. 5(a)). In this way, 2D beam-steering of the perovskite LEDs can be achieved by selecting the light emissions from different positions of PeNCs emitters integrated at the focal plane of the metalens. To understand our proposition, three points (denoted as "P_0", "P_1", and "P_2") at different locations of the PeNCs thin film were optically pumped in sequence by a focused 355 nm UV laser such that a small emitting beam with the size of approximately 5 μm × 5 μm can be created at the corresponding coordinates. The deflection angles of the generated beams were determined to be about 0°, 5.6°, and 7.4° along y-axis or x-axis, respectively, as shown in Figs. 5(b)–5(d), which agree well with the estimated values using Eq. (2) (see Fig. S10 in the ESM for measurement details).

Furthermore, as indicated in Eq. (2), the achievable range of the beam steering angles can be considerably extended by either employing a thinner sapphire substrate to reduce the f of the integrated metalens or increasing the size of metalens to allow the selection and operation of emitters in a larger area.

Note that in the proposed metalens-assisted beam steering system, the emitted light from the PeNCs thin film can be directed to a desired direction on an integrated optical chip by simply selecting different emitters. Therefore, by defining the perovskite thin film into micro-LEDs arrays at the focal plane of the integrated metalens, it will be possible to realize electrically controlled beam steering of LEDs though switching on/off different emitters with a fast modulation speed, which might find potential use in free-space optical communication applications without the requirements of mechanical movement parts.

3 Conclusions

In conclusion, this work developed a feasible and rather simple approach to integrate perovskite emitters with dielectric metasurface through one step spin-coating process for on-chip beam shaping. By doing this, it allows us to demonstrate directional emissions from perovskite emitters, including collimated light emissions and 2D beam steering. Notably, in the developed approach the light emitters were integrated on the back side of substrate after the fabrication of metasurface, it thus avoids the degradation of material optical quality that otherwise would have been caused by the multi-step nanofabrication. This is particularly beneficial for the optoelectronic applications of active materials that are sensitive and vulnerable to the chemical environments, like perovskites. Therefore, this work could serve as a generalized solution to combine the advantages of the latest dielectric metasurfaces, including the subwavelength compactness, high efficiency, and exceptional electromagnetic controllability, with the emerging perovskite based thin film LEDs. Moreover, our findings are readily to be extended to other solution processable materials, such as OLEDs and PLEDs, having the potential to promote the development of a new class of low-cost and ultra-compact solid state light sources with on-demand beam emitting characteristics.

4 Methods

4.1 Fabrication of GaN metalens

The GaN metalenses were fabricated using an electron beam lithography (EBL) system (JBX-5) 500ZA with metallic nickel (Ni) hard masks through a lift-off process. A 200 nm thick polymethyl methacrylate (PMMA) (AR-P 679.04) e-beam resist was spin-coated onto the GaN film, then baked at the temperature of 180 °C for 90 s. The sample was then exposed in the EBL system with an area dose 650 μC/cm^2 under 50 kV acceleration voltage. After development in MIBK/IPA (1:3) for 120 s and fixing in IPA for 30 s, a 50 nm thick Ni mask was deposited using E-beam evaporation. The lift-off process of the sample was done in the acetone solution for 10 min. Afterwards, the sample with the

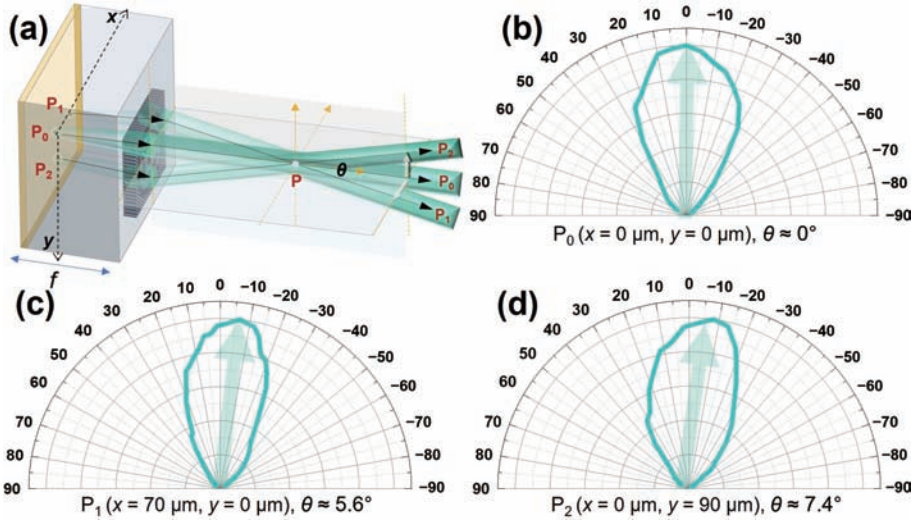

Figure 5 (a) Schematic illustration of the principle of metalense-assisted beam steering of perovskite emissions. (b)–(d) The polar representations of the measured beam intensity from the metasurface integrated perovskite emitters located at different positions of perovskite thin film, confirming the functionality of the proposed light emitting chip as a 2D beam steering device.

patterned Ni hard mask layer was etched by the inductively coupled plasma system (ICP) with the power of 300 W and a bias power of 50 W. Finally, the Ni mask on the top of GaN nanopillars was removed by chemical etching in 30% $FeCl_3$ solution.

4.2 Synthesis of perovskite thin film

The details of synthesis steps and the characterization results of the core–shell $FAPbBr_3$/$CsPbBr_3$ PeNCs thin film can be found in our previous study [29]. Briefly, FA-acetate, $Pb(CH_3COO)_2 \times 3H_2O$, oleic acid (OA), and ODE were first mixed inside a 100 mL flask, and dried at 50 °C in vacuum for 30 min. Then, the mixture was heated up to 130 °C under the protection of N_2 gas, followed by the injection of OAmBr in toluene. The reaction mixture was then cooled using ice-water bath. After that, the green solution of $FAPbBr_3$ NCs was collected, and stored at 4 °C. Then, $PbBr_2$, Cs_2CO_3, dried OA, ODE, OLA, and the as-synthesized $FAPbBr_3$ PeNCs were added into a 100 mL flask, and heated up to 80 °C in N_2 atmosphere, and then cooled down in the ice bath. Finally, the undispersed residue and aggregated PeNCs in the solution were removed using the centrifuge. The core–shell $FAPbBr_3$/$CsPbBr_3$ PeNCs were then dispersed in hexane and stored in the dark at 4 °C. For the integration with metasurfaces, the as-synthesized core–shell $FAPbBr_3$/$CsPbBr_3$ PeNCs were spin coated on the substrate at 2000 rpm for 60 s.

4.3 Optical characterization

The tests of metalens focal length and PL collimation were performed under a continuous-wave (CW) laser at 532 nm and a nanosecond pulsed UV laser at 355 nm, respectively. The signals were collected using a confocal microscopy system (Alpha300, WITec) with a 20× objective with the numerical aperture of 0.40. The angle-dependent PL spectra were measured by spectrometer (Andor SR-750-D1-R) equipped with a Newton charge-coupled device (CCD, model No. DU920P-BU).

Acknowledgements

This work is supported by the National Natural Science Foundation of China (Nos. 11804335, 61904017, 12074045, and 62174079) and Science, Technology and Innovation Commission of Shenzhen Municipality (Projects Nos. JCYJ20210324120204011 and KQTD2015071710313656). P. N. N. acknowledges the support of H2020 Research and Innovation Program (Marie Skłodowska-Curie Individual Fellowship; Agreement No. 101027383).

Electronic Supplementary Material: Supplementary material is available in the online version of this article at https://doi.org/10.1007/s12274-023-5439-y.

References

[1] De Almeida, A.; Santos, B.; Paolo, B.; Quicheron, M. Solid state lighting review—Potential and challenges in Europe. *Renewable Sustainable Energy Rev.* **2014**, *34*, 30–48.

[2] Crawford, M. H. LEDs for solid-state lighting: Performance challenges and recent advances. *IEEE J. Sel. Top. Quantum Electron.* **2009**, *15*, 1028–1040.

[3] Gather, M. C.; Köhnen, A.; Meerholz, K. White organic light-emitting diodes. *Adv. Mater.* **2011**, *23*, 233–248.

[4] Zhang, X. S.; Chen, Y. J.; Lian, L. Y.; Zhang, Z. Z.; Liu, Y. X.; Song, L.; Geng, C.; Zhang, J. B.; Xu, S. Stability enhancement of PbS quantum dots by site-selective surface passivation for near-infrared LED application. *Nano Res.* **2021**, *14*, 628–634.

[5] Giovanella, U.; Pasini, M.; Lorenzon, M.; Galeotti, F.; Lucchi, C.; Meinardi, F.; Luzzati, S.; Dubertret, B.; Brovelli, S. Efficient solution-processed nanoplatelet-based light-emitting diodes with high operational stability in air. *Nano Lett.* **2018**, *18*, 3441–3448.

[6] Li, Y.; Wang, X. Y.; Xue, W. N.; Wang, W.; Zhu, W.; Zhao, L. J. Highly luminescent and stable $CsPbBr_3$ perovskite quantum dots modified by phosphine ligands. *Nano Res.* **2019**, *12*, 785–789.

[7] Xiao, Z. G.; Kerner, R. A.; Zhao, L. F.; Tran, N. L.; Lee, K. M.; Koh, T. W.; Scholes, G. D.; Rand, B. P. Efficient perovskite light-emitting diodes featuring nanometre-sized crystallites. *Nat. Photon.* **2017**, *11*, 108–115.

[8] Cao, Y.; Wang, N. N.; Tian, H.; Guo, J. S.; Wei, Y. Q.; Chen, H.; Miao, Y. F.; Zou, W.; Pan, K.; He, Y. R. et al. Perovskite light-emitting diodes based on spontaneously formed submicrometre-scale structures. *Nature* **2018**, *562*, 249–253.

[9] Li, R. X.; Li, B. B.; Fang, X.; Wang, D. K.; Shi, Y. Q.; Liu, X.; Chen, R.; Wei, Z. P. Self-structural healing of encapsulated perovskite microcrystals for improved optical and thermal stability. *Adv. Mater.* **2021**, *33*, 2100466.

[10] Karunatilaka, D.; Zafar, F.; Kalavally, V.; Parthiban, R. LED based indoor visible light communications: State of the art. *IEEE Commun. Surv. Tutorials* **2015**, *17*, 1649–1678.

[11] Fu, X. Y.; Mehta, Y.; Chen, Y. A.; Lei, L.; Zhu, L. P.; Barange, N.; Dong, Q.; Yin, S. C.; Mendes, J.; He, S. L. et al. Directional polarized light emission from thin-film light-emitting diodes. *Adv. Mater.* **2021**, *33*, 2006801.

[12] Taki, T.; Strassburg, M. Review-visible LEDs: More than efficient light. *ECS J. Solid State Sci. Technol.* **2020**, *9*, 015017.

[13] Yu, N. F.; Genevet, P.; Kats, M. A.; Aieta, F.; Tetienne, J. P.; Capasso, F.; Gaburro, Z. Light propagation with phase discontinuities: Generalized laws of reflection and refraction. *Science* **2011**, *334*, 333–337.

[14] Lin, D. M.; Fan, P. Y.; Hasman, E.; Brongersma, M. L. Dielectric gradient metasurface optical elements. *Science* **2014**, *345*, 298–302.

[15] Yang, J. Y.; Gurung, S.; Bej, S.; Ni, P. N.; Lee, H. W. H. Active optical metasurfaces: Comprehensive review on physics, mechanisms, and prospective applications. *Rep. Prog. Phys.* **2022**, *85*, 036101.

[16] Liu, J. Y.; Duan, Y. P.; Zhang, T.; Huang, L. X.; Pang, H. F. Dual-polarized and real-time reconfigurable metasurface absorber with infrared-coded remote-control system. *Nano Res.* **2022**, *15*, 7498–7505.

[17] Brière, G.; Ni, P. N.; Héron, S.; Chenot, S.; Vézian, S.; Brändli, V.; Damilano, B.; Duboz, J. Y.; Iwanaga, M.; Genevet, P. An etching-free approach toward large-scale light-emitting metasurfaces. *Adv. Opt. Mater.* **2019**, *7*, 1801271.

[18] Yu, N. F.; Aieta, F.; Genevet, P.; Kats, M. A.; Gaburro, Z.; Capasso, F. A broadband, background-free quarter-wave plate based on plasmonic metasurfaces. *Nano Lett.* **2012**, *12*, 6328–6333.

[19] Wang, L.; Kruk, S.; Koshelev, K.; Kravchenko, I.; Luther-Davies, B.; Kivshar, Y. Nonlinear wavefront control with all-dielectric metasurfaces. *Nano Lett.* **2018**, *18*, 3978–3984.

[20] Teng, S. Y.; Zhang, Q.; Wang, H.; Liu, L. X.; Lv, H. R. Conversion between polarization states based on a metasurface. *Photon. Res.* **2019**, *7*, 246–250.

[21] Xie, Y. Y.; Ni, P. N.; Wang, Q. H.; Kan, Q.; Briere, G.; Chen, P. P.; Zhao, Z. Z.; Delga, A.; Ren, H. R.; Chen, H. D. et al. Metasurface-integrated vertical cavity surface-emitting lasers for programmable directional lasing emissions. *Nat. Nanotechnol.* **2020**, *15*, 125–130.

[22] Ni, P. N.; De Luna Bugallo, A.; Arellano Arreola, V. M.; Salazar, M. F.; Strupiechonski, E.; Brändli, V.; Sawant, R.; Alloing, B.; Genevet, P. Gate-tunable emission of exciton-plasmon polaritons in hybrid MoS_2-gap-mode metasurfaces. *ACS Photonics* **2019**, *6*, 1594–1601.

[23] Park, Y.; Kim, J.; Cho, K. S.; Kim, H.; Lee, M. K.; Lee, J. S.; Kim, U. J.; Hwang, S. W.; Brongersma, M. L.; Roh, Y. G. et al. Metasurface electrode light emitting diodes with planar light control. *Sci. Rep.* **2017**, *7*, 14753.

[24] Mao, P.; Liu, C. X.; Li, X. Y.; Liu, M. X.; Chen, Q.; Han, M.; Maier, S. A.; Sargent, E. H.; Zhang, S. Single-step-fabricated disordered metasurfaces for enhanced light extraction from LEDs. *Light Sci. Appl.* **2021**, *10*, 180.

[25] Iyer, P. P.; DeCrescent, R. A.; Mohtashami, Y.; Lheureux, G.; Butakov, N. A.; Alhassan, A.; Weisbuch, C.; Nakamura, S.;

DenBaars, S. P.; Schuller, J. A. Unidirectional luminescence from InGaN/GaN quantum-well metasurfaces. *Nat. Photonics* **2020**, *14*, 543–548.

[26] Khaidarov, E.; Liu, Z. T.; Paniagua-Domínguez, R.; Ha, S. T.; Valuckas, V.; Liang, X. N.; Akimov, Y.; Bai, P.; Png, C. E.; Demir, H. V. et al. Control of LED emission with functional dielectric metasurfaces. *Laser Photonics Rev.* **2020**, *14*, 1900235.

[27] Liu, S.; Vaskin, A.; Addamane, S.; Leung, B.; Tsai, M. C.; Yang, Y. M.; Vabishchevich, P. P.; Keeler, G. A.; Wang, G.; He, X. W. et al. Light-emitting metasurfaces: Simultaneous control of spontaneous emission and far-field radiation. *Nano Lett.* **2018**, *18*, 6906–6914.

[28] Dai, W.; Wang, Y. J.; Li, R. X.; Fan, Y. B.; Qu, G. Y.; Wu, Y. K.; Song, Q. H.; Han, J. C.; Xiao, S. M. Achieving circularly polarized surface emitting perovskite microlasers with all-dielectric metasurfaces. *ACS Nano* **2020**, *14*, 17063–17070.

[29] Zhang, X. Y.; Guo, Z. H.; Li, R. X.; Yu, J. H.; Yuan, B. Z.; Chen, B. A.; He, T. C.; Chen, R. Quasi-type II core–shell perovskite nanocrystals for improved structural stability and optical gain. *ACS Appl. Mater. Interfaces* **2021**, *13*, 58170–58178.

[30] Wang, Q. H.; Ni, P. N.; Xie, Y. Y.; Kan, Q.; Chen, P. P.; Fu, P.; Deng, J.; Jin, T. L.; Chen, H. D.; Lee, H. W. H. et al. On-chip generation of structured light based on metasurface optoelectronic integration. *Laser Photonics Rev.* **2021**, *15*, 2000385.

[31] Engelberg, J.; Zhou, C.; Mazurski, N.; Bar-David, J.; Kristensen, A.; Levy, U. Near-IR wide-field-of-view Huygens metalens for outdoor imaging applications. *Nanophotonics* **2020**, *9*, 361–370.

[32] Yang, W. H.; Xiao, S. M.; Song, Q. H.; Liu, Y. L.; Wu, Y. K.; Wang, S.; Yu, J.; Han, J. C.; Tsai, D. P. All-dielectric metasurface for high-performance structural color. *Nat. Commun.* **2020**, *11*, 1864.

[33] Chen, W. T.; Zhu, A. Y.; Capasso, F. Flat optics with dispersion-engineered metasurfaces. *Nat. Rev. Mater.* **2020**, *5*, 604–620.

[34] Kim, I.; Martins, R. J.; Jang, J.; Badloe, T.; Khadir, S.; Jung, H. Y.; Kim, H.; Kim, J.; Genevet, P.; Rho, J. Nanophotonics for light detection and ranging technology. *Nat. Nanotechnol.* **2021**, *16*, 508–524.